Proceedings of the XXVI International School of Semiconducting Compounds, Jaszowiec 1997

MAGNETOTRANSPORT AND MAGNETOOPTICS OF $InAs_{1-x}Sb_x$ AND HETEROJUNCTIONS COMBINATIONS FORMED BETWEEN InAs AND GaSb, AlSb OR $InAs_{1-x}Sb_x$

R.A. STRADLING

Blackett Laboratory, Imperial College of Science, Technology & Medicine
London SW7 2BZ, UK

Cyclotron resonance and interband measurements are reported in magnetic fields up to 160 T for $InAs/InAs_{1-x}Sb_x$ superlattices, one of which is a "self-organised" or "natural" superlattice, and $InAs_{1-x}Sb_x$ epilayers. The samples were grown by MBE at temperatures between 370°C to 500°C. No dependence of the band gap, effective masses or g-values on the growth temperature was detected. Anomalous tilt behaviour was observed for the superlattices. Inversion asymmetry induced spin-splitting of the subbands in gated InAs quantum wells is investigated by means of the Shubnikov–de Haas effect and cyclotron resonance. The non-parabolicity was well fitted by Kane theory, although the measured values of effective mass were substantially higher than predictions. Infrared life time measurements at wavelengths between 6 and 85 microns are undertaken with free electron lasers on $InAs/InAs_{1-x}Sb_x$ superlattices and InAs/AlSb quantum wells. Suppression of the Auger recombination times is demonstrated with the superlattices.

PACS numbers: 72.20.My, 76.40.+b, 78.20.Ls

1. Introduction

A series of magnetooptical and magnetotransport experiments of InAs/GaSb/AlSb quantum wells and $InAs_{1-x}Sb_x/InAs$ strained layer superlattices fabricated at Imperial College are discussed. A characteristic of the InAs/GaSb/AlSb combinations is their high mobility. By using gated structures the Fermi energy/electron concentration can be varied in arbitrarily small steps while leaving the main sample parameters unchanged.

The band offsets for the $InAs/InAs_{1-x}Sb_x$ superlattice system are the subject of some controversy with different groups variously putting forward type IIA and type IIB alignments. In one case type I alignment coupled with strong narrowing of the band gap induced by Cu–Pt ordering in the alloy has also been proposed. In view of this controversy cyclotron resonance and interband measurements were

undertaken with samples grown over a range of temperatures between 370°C to 500°C. Alloy ordering, clustering and other metallurgical artefacts such as phase separation occur over this temperature range and their magnitude changes strongly as the temperature is reduced.

The $InAs_{1-x}Sb_x/InAs$ strained layer superlattices have rather long non-radiative life times despite inferior structural quality as demonstrated by time resolved pump-probe measurements with a free electron laser. The long non-radiative life times appears to be associated with a type II band alignment and makes such structures interesting for infrared laser applications.

2. Cyclotron resonance of $InAs_{1-x}Sb_x$ epilayers and $InAs/InAs_{1-x}Sb_x$ superlattices

2.1. Introduction

The band offsets for the $InAs/InAs_{1-x}Sb_x$ superlattice system are the subject of some controversy with different groups variously putting forward type IIA and type IIB alignments [1, 2] on the basis of interband magnetoabsorption experiments performed at relatively low fields (< 10 T). In one case type I alignment coupled with strong narrowing of the band gap induced by Cu–Pt ordering in the alloy has also been proposed [3]. This work is now extended to include intraband studies and to fields where the Landau level energies in the conduction band become comparable to the conduction band offsets. Bulk $InAs_{1-x}Sb_x$ alloys are also investigated in order to determine any order induced narrowing of the band gap and the effects on the conduction band parameters.

2.2. Sample properties and experimental method

Significant alloy ordering and clustering is observed in transmission electron diffraction experiments [4] with our MBE samples grown below 450°C for $0.2 < x < 0.8$. The ordering becomes stronger as the growth temperature is reduced, reaching a maximum at about 400°C and below about 400°C phase separation occurs. Below this temperature and for $0.3 < x < 0.7$ a natural superlattice is formed during MBE growth by a form of self-assembly associated with the miscibility gap [5]. The mobilities are a strong function of growth temperature with the highest mobilities being obtained between 430°C and 470°C [6].

We report cyclotron resonance (CR) for one such natural superlattice ($InAs_{0.7}Sb_{0.3}/InAs_{0.3}Sb_{0.7}$) and compare the results with those for a conventional superlattice ($InAs/InAs_{0.8}Sb_{0.2}$). All samples with the exception of the conventional superlattice were n-type without deliberate doping. With the conventional superlattice a thick strain-matched buffer of composition $InAs_{0.9}Sb_{0.1}$ was doped with 2×10^{17} cm^{-3} Be acceptors in order to prevent any interfering electron CR signal from this region and the 100 period superlattice was doped with 1×10^{17} cm^{-3} Si donors. The sample parameters and the CR conclusions discussed in Sec. 2.2 are summarised in Table. The experimental methods are discussed in Ref. [7] and some preliminary results were given in Ref. [8].

TABLE

Summary of samples investigated by cyclotron resonance and the band-edge effective masses and g-values measured.

Sample No.	x	T_g [°C]	d [μm]	Mobility (300 K) [m^2 V s]	n (300 K) [$\times 10^{22}$ m^{-3}]	m_0^*/m (1)	$\lvert g_0^*\rvert$ (1)	m_0^*/m (2)	$\lvert g_0^*\rvert^*$ (2)
InAs	0	490	10	2	1	0.0217	30	0.0222	30
119	0.2	370	4.3	0.44	21	0.0157	40	0.0165	40
610	0.32	500	1	0.29	38	0.0127	55	0.0137	54
606	0.46	470	1	1.0	13	0.0095	79	0.0106	75
614	0.52	440	1	0.7	14	0.0090	82	0.0099	79
218	0.71	430	3.2	1.6	11	0.0088	98	0.0099	92
121	0.86	370	4.23	0.85	7	0.0102	103	0.0111	101
InSb	1					0.0125	89	0.0133	88
576	0/0.2 SLS	450	4.4	1.5	20	0.02			
110	0.6 0.4/0.8 NSLS	370	3.3	0.2	42	0.035			

(1) assumes $E_g(300\ \mathrm{K}) = E_g(0) - 20$ meV whereas (2) assumes $E_g(300\ \mathrm{K}) = E_g(0)$. SLS = strained layer superlattice, NSLS = natural SLS, all on GaAs substrates.

2.3. Experiments with bulk $InAs_{1-x}Sb_x$ alloys

Figure 1 shows a "fan-chart" for $x = 0.71$ and a laser wavelength of 10.6 μm of the magnetic fields at which the cyclotron resonance is observed at 300 K for the two spin orientations together with the lowest energy interband transition. The quantum limit applies at low temperatures; i.e. all carriers are in the $n = 0$, lower spin state so the upper of the two CR transitions disappears. Figure 2a shows the effective mass ratios (m^*/m) against alloy composition (x) obtained at room temperature at 10.6 μm.

Extrapolation of the energy of the interband transition back to zero field for the sample with $x = 0.71$ provides a rather accurate value for the room temperature energy gap of 86.0 ± 1.5 meV. A similar procedure for the samples with $x = 0.50$ and 0.55 gives $E_g = 99.9$ and 90.6 ± 1.5 meV. Extrapolation of the temperature shifts observed on the interband transition gives -47 ± 5 meV for the shift of the gap from 80 K to 300 K. Thus the low temperature values for the gap are estimated to be 133, 137.5 and 147 meV for $x = 0.71, 0.52$ and 0.46, respectively. The band gap shows very strong band bowing as a function of x. Interband magnetooptics has been performed on similar samples [9]. From the formula given in Ref. [9] the minimum gap is estimated to be 128 meV and to occur at $x = 0.63$. An average of other literature values give a minimum of 146 ± 10 meV at $x = 0.64 \pm 0.01$. Thus no dependence could be detected of the band gap or

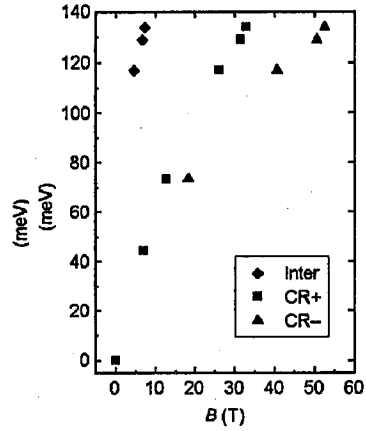

Fig. 1. Energy transitions (in meV) of the two spin-split cyclotron resonance and the lowest energy interband transition against B (in T) for sample 218 at 300 K and 10.6 μm wavelength.

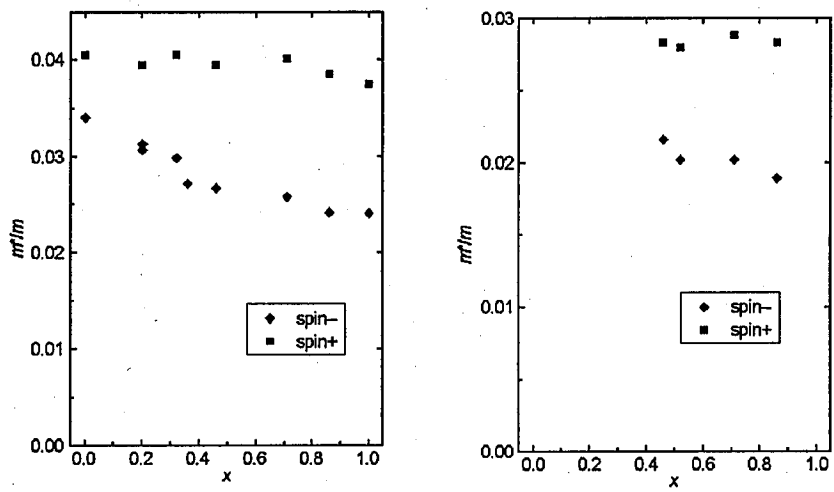

Fig. 2. (m^*/m) vs. x for spin-up and spin-down CR lines at (a) 10.6 μm, (b) 16.9 μm wavelength, respectively.

other band parameter on the growth temperature which varied between 430°C and 500°C. Any order-induced band gap narrowing in these MBE-grown samples must be smaller than about 15 meV even in the mid-gap region. It should be recalled however that the interband experiments suggesting an order induced band gap narrowing [3] were performed with MOVPE samples. The ordering measured in TED experiments with MOVPE samples appears to be stronger than with MBE material and to occur at higher growth temperatures.

The effective masses obtained increase rapidly with decreasing laser wavelength (increasing field) as expected for highly non-parabolic bands as can be seen from a comparison of Figs. 2a and b. In order to model the cyclotron resonance transitions, we employ a formula originally used by Palik et al. [10] to describe the cyclotron resonance transition energies ($y_\pm = 2E_\pm/E_g$) in bulk InAs up to 10 T

$$y_\pm = [1 + b_{n+1,\pm}x]^{\frac{1}{2}} - [1 + b_{n,\pm}x]^{\frac{1}{2}},$$

where

$$b_{n,\pm} = 4\left(n + \frac{1}{2} \pm \frac{1}{4}g_0^* m_0^*\right) \quad \text{and} \quad x = \frac{\hbar eB}{E_g m_0^*}.$$

In this approach the three main variables are the band gap (E_g) and the band edge mass (m_0^*) and g-value (g_0^*) which appear in the dimensionless parameters and $x = \hbar\omega_0/E_g$ and $\delta = (g_0^* m_0^*/m)$. One problem in fitting the data is to determine the value of the effective band gap to use at room temperature as only the dilational component of the reduction in E_g with increasing temperature will change the effective mass. We assume in our fit to the data that this amounts to a constant reduction of 20 meV to the low temperature values derived in Ref. [9]. The parameters m_0^*/m and g_0^* are used to fit the effective masses determined at several different wavelengths. Table lists the m_0^*/m and g_0^* parameters derived in this way (data set 1) and also for comparison the values derived assuming that the low temperature band gap should be applied (data set 2). Figures 3a and b plot the results as a function of alloy composition (x).

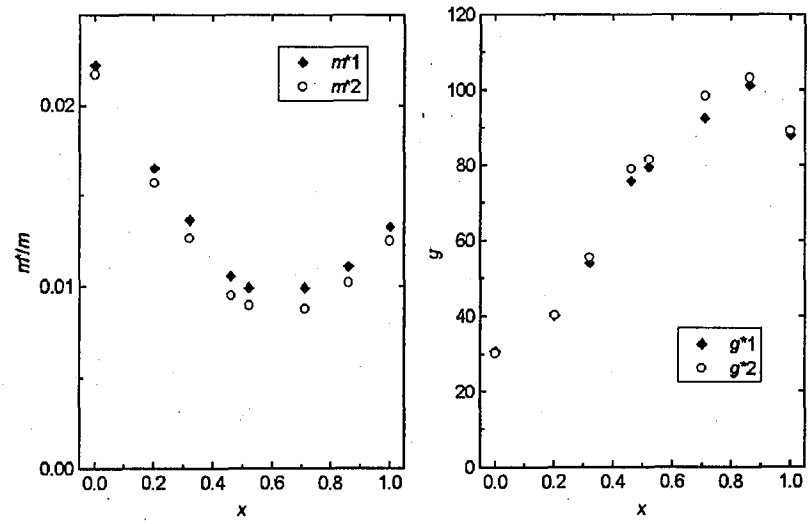

Fig. 3. (a) band edge effective mass (300 K) and (b) band edge effective g-value (300 K) versus alloy composition (x) assuming (1) that the dilatational change in the band gap corresponds to 20 meV and (2) with the low temperature band gap as discussed in the text.

2.4. Experiments with the $InAs/InAs_{1-x}Sb_x$ superlattice system

The CRs for the self-assembled "natural superlattice" are the first measurements for such a system. The sample was grown at 370°C. Transmission electron diffraction experiments [5] gave the compositions of the two phases as 0.42 and 0.80 and the size of the platelet s forming the superlattice as 1200×500 nm^2 in lateral dimensions with a thickness of 35 nm. The effective masses ratios are much higher than those measured for the bulk alloy systems and change much less with laser wavelength (e.g. low temperature values of 0.0405 for 10.6 μm and 0.0365 for 28 μm wavelength compared with 0.0267 and 0.0187 measured at 10.6 and 28 μm for a homogeneous bulk sample of the same nominal composition of $x = 0.6$). The behaviour found on tilting the magnetic field is highly anomalous with the main CR peak shifting downwards for 10.6 μm on increasing the tilt angle (reaching a shift of −33% at a tilt angle of 30°) but rapidly upwards at roughly three times the $1/\cos\theta$ rate at 16.9 μm (+45% at 30° tilt) (see Fig. 4). In addition a much weaker peak which is nearly independent of tilt angle is seen. At 28 μm the shift is upwards at a rate of $1.5 \times (1/\cos\theta)$. This behaviour is consistent with an anticrossing interaction with a higher miniband centred at about 60 meV above the lowest energy subband. Similar anticrossing behaviour was recently reported in tilted cyclotron resonance experiments with InAs/GaSb superlattices [11].

Qualitatively different tilt behaviour is found with the $InAs/InAs_{0.8}Sb_{0.2}$ superlattice (Fig. 5). For laser wavelengths of 16.9 and 10.6 μm, the $n = 0- \rightarrow 1-$ peak moves down in magnetic field at the same rate (22% for 60° tilt). For 5.53 μm,

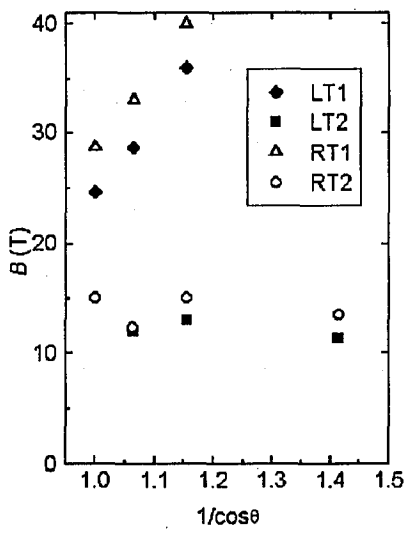

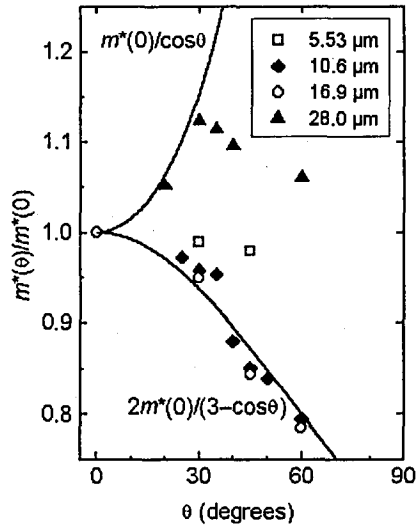

Fig. 4. The tilt behaviour found with the $InAs/InAs_{0.8}Sb_{0.2}$ superlattice at 16.9 μm wavelength.

Fig. 5. The shift of the cyclotron resonance peak with tilt angle for four different wavelengths.

the peaks are almost isotropic. At 28 μm the shift is at first upwards as $1/\cos\theta$, reaching +12% at 30° but then the shift reduces to +5% at 60°. These observations are consistent with a simple model where it is assumed that the $n = 1$ Landau level lies above the top of the quantum well for $B > 15$ T whereas the $n = 0$ level is confined for $B < 40$ T but becomes progressively unconfined at higher fields. This model predicts a shift downwards which is given by $2/(3 - \cos\theta)$ which is close to that observed experimentally at 16.9 and 28 μm wavelengths. Further experiments are needed to confirm the details of the tilt behaviour and the influence of any anticrossing effects between states from different minibands.

2.5. Discussion

The data presented in Figs. 2–3 and Table represent an extensive study of the conduction band masses and g-values for the full range of alloy compositions. In the case of the band-edge effective mass ratios the values for the binaries are close to those derived from other techniques at comparable temperatures; e.g. 0.01274 at 160 K for InSb and 0.0240 at 110 K for InAs [12]. The momentum matrix elements (E_p) required to fit the band edge effective masses are shown in Fig. 6. The values of E_p are almost identical to those found from interband magnetooptics [9]; e.g. 16 eV for $x = 0.5$ compared with 15.5 eV quoted in Ref. [9]. However the g-values are larger than expected: $|g_0^*| = 30$ for InAs compared with 17.5 (300 K) [13] and $|g_0^*| = 89$ compared with 51.3 (60 K) [13] for InSb. Both the effective masses and g-values quoted in Table are relatively insensitive to the precise value of band gap assumed. The results for the $|g_0^*|$ values therefore show that the differences

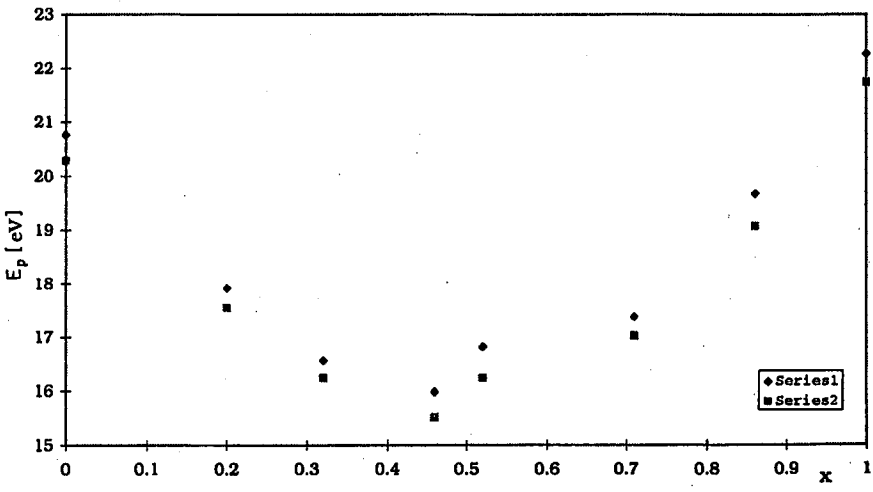

Fig. 6. The momentum matrix elements (E_p) against alloy composition (x) calculated for room temperature assuming (1) that the dilatational change in the band gap corresponds to 20 meV and (2) with the low temperature band gap as discussed in the text.

between the spin-up and spin-down energies/fields are larger than anticipated. This difference probably arises from corrections to the two-band treatment at the rather high photon energies involved.

It has been shown that the tilt behaviour of the intraband cyclotron resonance can provide information on the band offsets, thereby avoiding the sophisticated band structure calculations required to interpret interband measurements.

3. Investigation of inversion asymmetry effects and conduction band nonparabolicity in gated InAs/GaSb quantum well structures

3.1. Introduction

By using gated structures the Fermi energy/electron concentration can be varied in arbitrarily small steps while leaving all other sample parameters unchanged.

The four wafers used to fabricate the MOS structures were grown by molecular beam epitaxy at 450°C on to semi-insulating GaAs substrates. 800 nm of GaSb was followed by a single InAs quantum well of thickness 20 nm with InSb interfaces and completed with a cap of 20 nm of GaSb. Mesas for the Hall bars were defined photolithographically. Capacitor or MOS structures were formed by depositing between 80 and 100 nm of SiO_2, either by plasma enhanced CVD or by a low temperature photolytic process followed by a Ni/Cr/Au gate. With these sample parameters the intrinsic electron concentration in the well at low temperatures generated by transfer from the GaSb valence band is 0.4×10^{12} cm^{-2} and surface donors generate an additional 0.5×10^{12} cm^{-2}. The variation in carrier concentration (n) with bias before the oxide broke down was typically from 0.8 to 3×10^{12} cm^{-2} (i.e. $+2 \times 10^{12}$ cm^{-2} electrons could be added by employing the gated structure). Despite the presence of surface donors, the observed (dn/dV) measured for the structures were within a factor of two of the values predicted by modelling assuming no interface states.

Electron concentrations as high as 3×10^{12} cm^{-2} can be generated in the gated samples. In order to distinguish between effects which are simply related to changes in the carrier concentration/Fermi energy and those explicitly related to the application of an electric field, the results are compared with those for an ungated sample where the electric field averaged over the well is designed to be near zero.

3.2. Inversion asymmetry splittings observed in the Shubnikov–de Haas effect

A strong beating pattern is superimposed at relatively low fields on the Shubnikov–de Haas (Sh–dH) peaks (see Fig. 7). Similar beating patterns have been reported previously for ungated InAs/GaSb quantum wells [14], for gated HgTe quantum wells [15, 16], and for GaAs/AlGaAs [17] and InGaAs/AlInAs heterostructures [18]. In Ref. [14, 15, 17] the beating was attributed to spin–orbit (S–O) induced terms [19, 20] (a "k^3" term arising from the lack of inversion symmetry in the bulk material and the k-dependent "Rashba" term). Structural inversion asymmetry can also induce zero-field spin-splitting of the subbands [21].

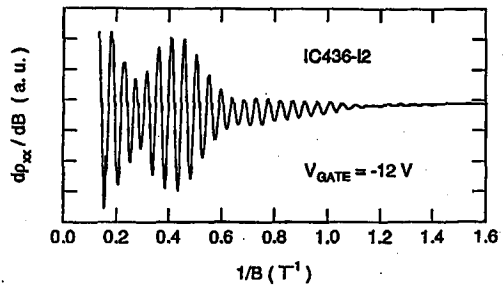

Fig. 7. The differential of the resistance against inverse magnetic field (sample IC436-12) at –12 V gate bias.

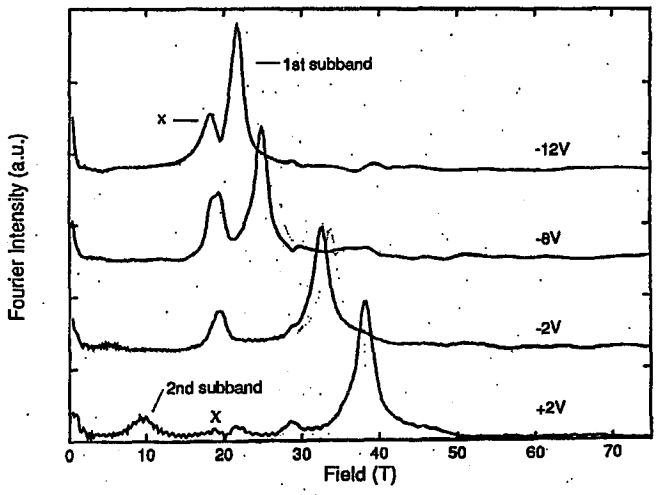

Fig. 8. Several Fourier transforms of the Shubnikov–de Haas oscillations for different gate voltages (sample IC436-12).

In the case of the GaAs/AlGaAs structures [17], the beating structure was believed to result from the occupancy of the second subband. Such beating patterns can also arise from resonant magneto-intersubband scattering (MIS) which occurs when Landau levels from different subbands become degenerate [22].

Fourier analysis of the Shubnikov–de Haas peaks showed an additional peak marked X in Fig. 8 which splits off from the main Fourier peak as the gate bias is increased. At a gate voltage of about –2 V occupancy of the second subband also becomes apparent. A weak second harmonic of the strongest peak and sum and difference peaks arising from mixing between the first and second subband occupancies are observed at positive gate voltages. The intensity of peak X relative to the main peak in the Fourier spectrum is strongly dependent on the field range sampled as can be seen from Fig. 9. In Ref. [14] a similar switch in relative intensity of the low and high field series was reported.

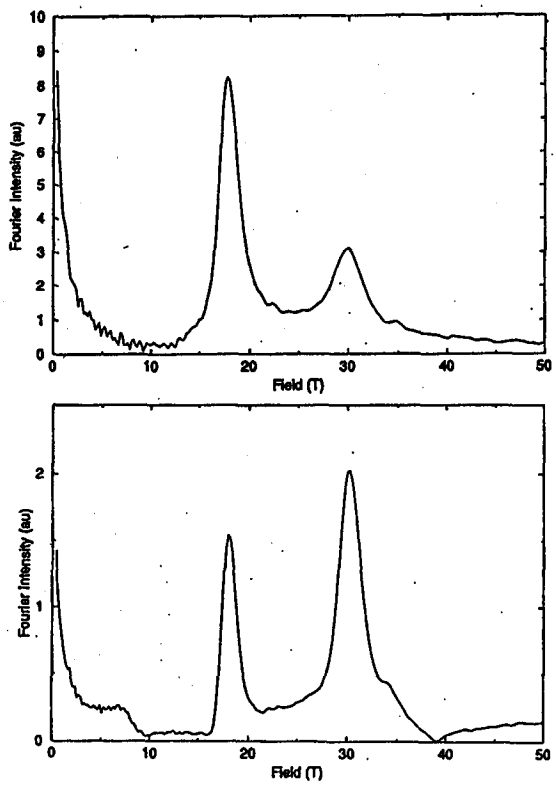

Fig. 9. The Fourier transform for a gated sample (450 h) sampled over a field range from 0.1 to 2 T in comparison with that for 0.1 to 6 T.

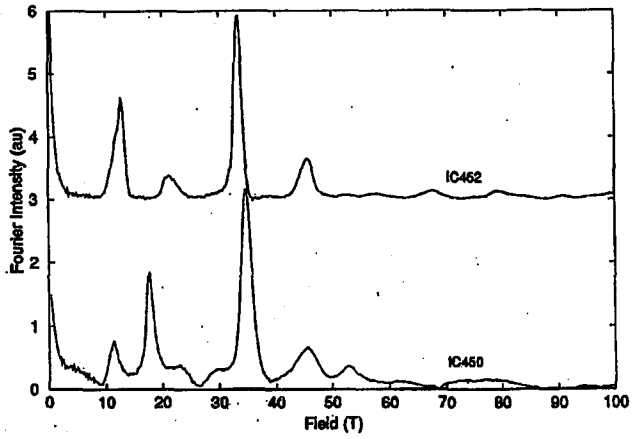

Fig. 10. The Fourier transforms for a gated sample (450 h) in comparison with that for an ungated modulation-doped sample (452).

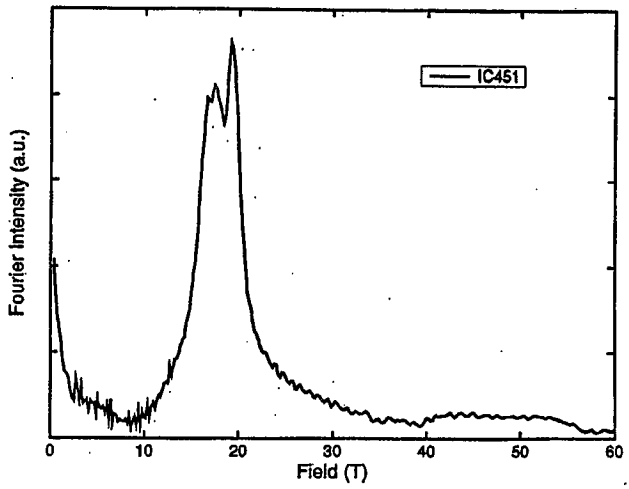

Fig. 11. The largest spin–orbit induced splitting of the Fourier transform found for an ungated sample.

These observations alone do not allow us to distinguish between the various mechanisms involving inversion asymmetry, MIS and Sh–dII from the second subband. However comparison with the results for ungated modulation-doped samples demonstrates that an inversion asymmetry mechanism is dominant. The potential in the well of these modulation-doped samples is engineered to be symmetric by locating the doping spike on the opposite side of the quantum well to the surface donors [23]. Figure 10 unambiguously shows that line X is absent in such a sample. With ungated samples without modulation-doping the electric field from the surface donors generally produces a beating pattern but with far smaller splittings in the Fourier spectra (Fig. 11 shows the largest splitting observed for an ungated sample with a 20 nm GaSb cap).

3.3. Cyclotron resonance with the gated structures

Cyclotron resonance was used to monitor the field effect in the gated structures and to determine the electron effective mass at high carrier densities. The carrier concentrations derived from the Shubnikov–de Haas effect, from the multiple carrier fits to the magnetoresistance and from the cyclotron resonance were all in agreement to a few percent. The effective mass ratios (m^*/m) were the same at the same carrier concentration for gated and modulation-doped samples (Fig. 12) but the m^*/m values for samples with AlSb barriers were slightly higher for the same carrier concentration. The observed values were consistently above the predictions of Kane theory although the change in mass due to non-parabolicity agreed well with the theory. Inclusion of strain makes the disagreement worse as can be seen from Fig. 12. Wave function penetration into the barriers also cannot explain the observations.

Despite the large inversion asymmetry splittings observed in the Sh–dH effect the CR line did not show splittings of comparable magnitude. Weak splittings were

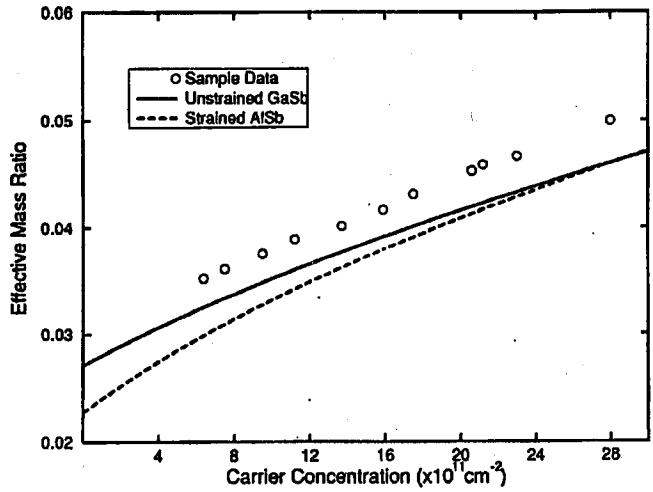

Fig. 12. (m^*/m) against carrier concentration. Full and dotted lines show the Kane predictions assuming no strain and the strain for AlSb barriers.

observed but these had the values predicted for the differences in energy between the transitions involving different Landau indices (i.e. $n-1$ to n and n to $n+1$) due to the band non-parabolicity evident in Fig. 12. An explanation for the failure of the CR to exhibit a strong Rashba or structural asymmetry effect could lie in a type of "motional narrowing" occurring for high mobilities (150000 $cm^2/(V\ s)$ in the present structures) similar to that discussed in Ref. [24].

3.4. Discussion

The strong electric-field related splitting of the Shubnikov–de Haas series observed is consistent with the presence of very few interface states either between the SiO_2 and the GaSb or at the InAs quantum well. The magnitude of the splittings is of the order of the value predicted for the Rashba effect [19, 20] (1.1×10^{11} meV cm^2).

4. Measurements of the life times of photoexcited carriers using a Free Electron Laser

Free Electron Lasers (FELs) offer an unrivalled combination of wide, rapid and continuous tunability, high peak power ($\approx$ 1 MW cm^{-2}) and controlable high (ps) time resolution. In the far infrared (FIR) region other systems give only sparse coverage and do not have the time resolution. The Dutch FEL at Utrecht (FELIX), is a unique facility, giving laser output for time resolved spectroscopy spanning the 5 to 110 μm wavelength range. Using FELIX we have carried out both saturation absorption and time-resolved measurements of $InAs/InAs_{1-x}Sb_x$ strained layer superlattices (SLS) grown by MBE which show the very high luminescence efficiencies between 4 and 11 microns. These structures have band gaps which match the wavelengths available from FELIX. We first observed a

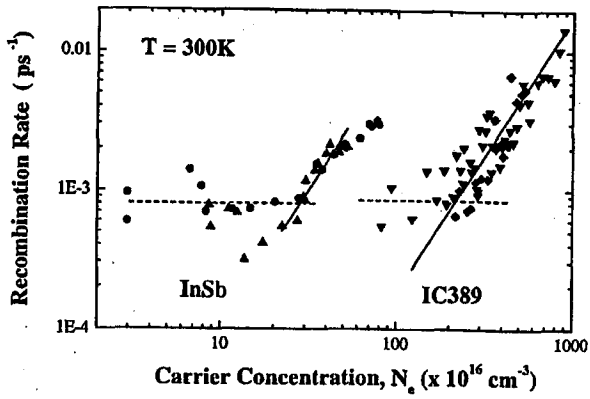

Fig. 13. The recombination rates in ps as measured as a function of excited carrier density in an infrared pump-probe experiment on an $InAs/InAs_{0.6}Sb_{0.4}$ strained layer superlattice (IC389) grown by MBE in comparison with the rates for an InSb sample, also grown by MBE.

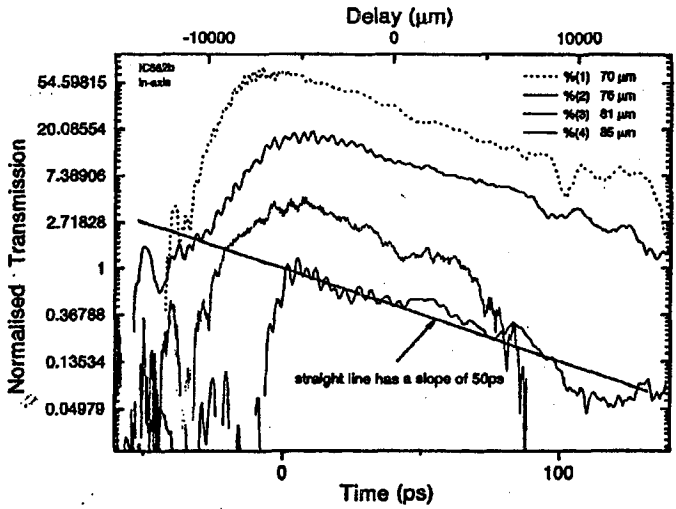

Fig. 14. The normalised transmission as a function of delay time in pump-probe cyclotron absorption experiments with an InAs/AlSb single quantum well sample for wavelengths between 70 and 85 microns as a function of delay time in picoseconds.

dramatic bleaching of interband absorption for these structures [25]. This is consistent both with the extremely strong room temperature photoluminescence discussed above and with suppression of the Auger processes by "band structure engineering". We then moved on to pump-probe experiments [26] which measure directly the room temperature life time of an $InAs/InAs_{1-x}Sb_x$ SLS [25]. Using the FEL it was possible to obtain results over a much wider range of excited carrier densities, N_e, than obtained previously by less direct methods. The different

scattering regimes were clearly distinguished, as can be seen from Fig. 13 from Shockley–Read (carrier concentration independent) life times at low excitation intensity, through an N_e-squared dependence at intermediate concentrations consistent with non-degenerate Auger scattering, to a linear N_e dependence at high concentrations, as expected for degenerate Auger scattering.

In comparison with the Auger life time obtained from similar measurements on InSb (room temperature band gap about 7 μm), the life time deduced from an alloy, whose measured band gap was 11 μm, was an order of magnitude longer (Fig. 13). These measurements represent the longest room-temperature life time yet measured for a III–V semiconductor, either in bulk or heterostructure form.

We are also undertaking cyclotron resonance measurements with high mobility ($\approx$ 250000 cm^2/(V s)) InAs/AlSb quantum wells. Here, in collaboration with Prof. C.R. Pidgeon of Heriot–Watt University and the FOM Plasma Institute in Utrecht which houses the Free Electron Laser "FELIX", we have performed the first ps pump-probe measurements at far infrared wavelengths (70 to 85 μm). The directly measured life time of the Landau levels is $\approx$ 50 ps at 4 K (Fig. 14).

Acknowledgments

This paper summarises the work of many colleagues; I am particularly grateful to H. Arimoto, S.J. Chung, C.M. Ciesla, I. Galbraith, D.A. Jaroszynski, C. Langerak, M. Livingstone, T. Malik, N. Miura, B.N. Murdin, J. Nehls and A.G. Norman, C.C. Phillips, C.R. Pidgeon, W.T. Yuen.

References

[1] P.J.P. Tang, M.J. Pullin, S.J. Chung, C.C. Phillips, R.A. Stradling, A.G. Norman, Y.B. Li, L. Hart, *Semicond. Sci. Technol.* **10**, 1177 (1995).

[2] Y.B. Li, D.J. Bain, L. Hart, M. Livingstone, C.M. Ciesla, M.J. Pullin, P.J.P. Tang, W.T. Yuen, I. Galbraith, C.C. Phillips, C.R. Pidgeon, R.A. Stradling, *Phys Rev B* **55**, 4589 (1997).

[3] S.R. Kurtz, L.R. Dawson, R.M. Biefeld, D.M. Follstaedtt, B.L. Doyle, *Phys. Rev. B* **46**, 190 (1992).

[4] T.Y. Seong, A.G. Norman, J.L. Hutchison, I.T. Ferguson, G.R. Booker, R.A. Stradling, B.A. Joyce, Ed. A.G. Cullis, *Institute of Physics Conference Series* Vol. 117, IoP Publ., Bristol 1991, p. 485.

[5] A.G. Norman, T.Y. Seong, I.T. Ferguson, G.R. Booker, B.A. Joyce, *Semicond. Sci. Technol.* **8**, S9 (1993).

[6] R.A. Stradling, *Semicond. Sci. Technol.* **6**, C52 (1991).

[7] N. Miura, *High Magnetic Fields in Semiconductor Physics II*, Ed. G. Landwehr, in *Springer Series in Solid State Science*, Vol. 87, Springer, Berlin 1988, p. 618.

[8] R.A. Stradling, T.A. Malik, J. Plumridge, W.T. Yuen, N. Miura, H. Arimoto, Y. Imanaka, in: *Proc. XXIIIrd ICPS (Berlin) Pub*, Eds. M. Scheffler, R. Zimmerman, World Scientific, Singapore 1997, p. 2223.

[9] S.N. Smith, C.C. Phillips, R.H. Thomas, R.A. Stradling, I.T. Ferguson, A.G. Norman, B.N. Murdin, C.R. Pidgeon, *Semicond. Sci. Technol.* **7**, 900 (1992).

[10] E.D. Palik, G.S. Picus, S. Teitler, R.F. Wallis, *Phys. Rev.* **122**, 475 (1961).

[11] G.M. Summers, R.J. Nicholas, N.J. Mason, P.J. Walker, Y. Imanaka, H. Arimoto, N. Miura, in: *Proc. 12th Int. Conf. on High Magnetic Fields in the Physics of Semiconductors*, Eds. G. Landwehr, W. Ossan, World Scientific, Singapore 1997, p. 801.

[12] R.A. Stradling, R.A. Wood, *J. Phys. C* **1**, 1711 (1968).

[13] Landolt, Börnstein, *Numerical Data and Functional Relationships in Science and Technology, New Series III/22a*, Eds. G. Harbeke, O. Madelung, U. Rossler, Springer-Verlag, Berlin 1987, p. 126, 299.

[14] J. Luo, H. Munekata, F.F. Fang, P.J. Stiles, *Phys. Rev. B* **41**, 7685 (1990).

[15] M. Schultz, F. Heinrichs, U. Merkt, T. Colin, T. Skauli, P. Helgesen, S. Lovold, *Semicond. Sci. Technol.* **11**, 1168 (1996).

[16] M. Schultz, F. Heinrichs, A. Eckstein, U. Merkt, T. Colin, T. Skauli, S. Lovold, in: *Proc. 12th Int. Conf. on High Magnetic Fields in the Physics of Semiconductors*, Eds. G. Landwehr, W. Ossan, World Scientific, Singapore 1997, p. 817.

[17] T.P. Smith, F.F. Fang, U. Meirav, M. Heiblum, *Phys. Rev. B* **38**, 12744 (1988).

[18] B. Das, S. Datta, R. Reifenberger, *Phys. Rev. B* **41**, 8278 (1990).

[19] E.A. de Andrada e Silva, *Phys. Rev. B* **46**, 1921 (1992).

[20] E.A. de Andrada e Silva, G.C. La Rocca, F. Bassini, *Phys. Rev. B* **50**, 8523 (1994).

[21] P. Pfeffer, W. Zawadzki, *Phys. Rev. B* **52**, 14332 (1995).

[22] T.H. Sander, S.N. Holmes, J.J. Harris, D.K. Maude, J.C. Portal, *Surf. Sci.* **361/362**, 564 (1996).

[23] T. Malik, S. Chung, J.J. Harris, A.G. Norman, R.A. Stradling, W.T. Yuen, in: *Int Conf. on Narrow Gap Semiconductors (Santa Fe)*, Ed. J.L. Reno, IoP Conference Series, Vol. 144, IoP Publ., Bristol 1995, p. 229.

[24] N.R. Cooper, J.T. Chalker, *Phys. Rev. Lett.* **72**, 2057 (1994).

[25] B.N. Murdin, C.R. Pidgeon, D.A. Jaroszynski, C.C. Phillips, R.A. Stradling, C.M. Ciesla, R. Praseres, G.J.G.M. Langerak, in: *Int. Conf. on Narrow Gap Semiconductors (Santa Fe)*, Ed. J.L. Reno, IoP Conference Series, Vol. 144, IoP Publ., Bristol 1995, p. 267.

[26] B.N. Murdin, C.R. Pidgeon, R.A. Stradling, C.C. Phillips, C.M. Ciesla, M. Livingstone, I. Galbraith, D.A. Jaroszynski, G.J.G.M. Langerak, *J. App. Phys.* **80**, 2994 (1996).